Chapter 6

Summary and Recommendations

The results presented in this thesis provide powerful conclusions regarding animal-fluid interactions in their natural environment. However, as with most original works, many questions remain. We have shown that measurements of in situ flows are necessarily assumed to be two dimensional due to the inherent difficulties of three-dimensional quantification of flows. Since this assumption cannot always be made, especially of turbulent background flows in the ocean, a technique that measures three-dimensional flows in the field is necessary. We have also showed striking images of animal-induced fluid transport in situ that are described by the drift mechanism and compared these measurements with simulations of moving, passive particles. However, the interaction of unsteady animal motion and wake generation with the drift volume needs to be investigated. Depending on the animal's morphology or swimming mode, there may be a limiting characteristic that selects drift as a dominant mechanism of mixing over wake mixing and vice versa. Finally, multiple-animal interactions and its inherent effect on fluid transport needs to be extended to global scale ocean mixing, and its subsequent impact on climate needs to be addressed.

6.1 Further Development of SCUVA

6.1.1 Capturing Three-Dimensional Flow Fields

The primary limitation of SCUVA is its inability to measure three-dimensional flows. This challenge is general to the field of fluid flow measurement as a whole. Work is underway to apply recently

developed defocusing DPIV techniques [98] in order to enable three-dimensional measurements using SCUVA. There exists several particle-tracking velocimetry (PTV) algorithms that can be used. The primary difference between DPIV and PTV methods is in the spatial resolution of the measurements. Three-dimensional particle tracking can be achieved by changing the source of illumination from a planar sheet to a conical volume of light by careful selection of beam optics. The three-dimensional position of each particle can be determined by using a defocusing mask placed directly in front of the camera. The mask contains a pattern of three holes through which light can pass through to the CCD array of the camera. A raytracing algorithm is then used to correlate the particle image formed from light passing through each of the pinholes to the position of that particle in space. An important benefit of this technique is that it requires relatively little modification of the current SCUVA hardware configuration.

After preliminary testing, we designed a two-camera housing that does not require a defocusing mask (figure 6.1). The camera housings (Amphibico Incorporated) are attached to each other and separated by a known distance. The video cameras (Sony HDR-HC7) are operated simultaneously with a single controller by use of an internal cable. Volumetric illumination is provided by two HID light systems attached to each camera housing (Light and Motion) with variable light settings. The ability to make three-dimensional measurements significantly expands the range of scientific questions that can be addressed using SCUVA, especially those related to animal-fluid interactions in complex flow environments.

6.1.2 Correcting Flow Fields with Onboard Accelerometry

Traditional flow measurements in the laboratory require the camera to be stationary, and if the camera moves, its motion is known. This condition ensures that all of the measured flow is due to the particle motion relative to the camera and not due to the camera motion. In the field, SCUVA is operated by a single scuba diver who is often free-floating in the water column without physical attachments to the surface or bottom. There is likely to be some motion of the camera despite the efforts of the diver to remain motionless. Hence, the measured flow field will also include the

Figure 6.1. The most recent design iteration of SCUVA incorporates two video camera housings separated by a fixed distance with multiple-level HID lights, which allows for the capture of three-dimensional particle trajectories.

error introduced from camera motion (see section 2.2.2). If left uncorrected, the error due to camera motion may obscure the flow of interest. To account for camera motion, it is necessary to monitor the acceleration of the camera while images are being recorded. This motion can then be subtracted from flow measurements either in real-time or in subsequent post-processing. By adding a microprocessor accelerometer to the camera housing and synchronizing the accelerometer measurements with the timing of data collection, the camera motion can be removed from the flow measurements. This added feature will not only increase the measurement efficiency of flows generated by swimming animals (since a candidate data set does not require motionless conditions) but also allow for use of SCUVA as a profiling device. In oceanography, field measurements of turbulent fluid motions are conducted with CTD, shear, and microstructure profilers. Since these measurement techniques are limited to two dimensions, the assumption of isotropic turbulence is commonly used. By using SCUVA as a profiler, we can conduct measurements of turbulence without assuming isotropy.

6.2 Determining R_f of Swimming Animals Using Available Quantitative Data

As discussed in section 4.2, mixing efficiency is defined in stratified flows by the flux Richardson number (R_f). The mixing efficiency of a particular mixing process is measured by the resultant change in potential energy state of the fluid due to mechanical energy imparted to the flow to create mixing. In the case of swimming animals, the mechanical energy in the flow available for mixing is the wake kinetic energy. Collaborators studying jellyfish, copepod and krill swimming have compiled quantitative flow measurements of the wakes generated by these animals across species, animal morphologies, and swimming modes. However, use of this data to quantify R_f is limited since the data neglects the physical properties of the flow (i.e., density), which is a necessary component to determine the mixing efficiency. However, using the buoyancy simulations discussed in section 5.2.2, we can estimate the displacement of Lagrangian fluid particles with a given density in a stratified fluid to determine the change in potential energy due to an animal's swimming motions.

Depending on the degree of stratification simulated and animal swimming characteristics, fluid particles will be displaced after an animal swims through them. The vertical velocity of Lagrangian fluid particles is now defined as a function of the flow field generated by the animal ($\mathbf{u}_{animal}$, instead of the motion of a sphere as in equation 5.7)

$$\begin{aligned} u_x &= u_{x,animal}, \\ u_z &= u_{z,animal} + \frac{b}{N}, \end{aligned} \tag{6.1}$$

where N is the buoyancy frequency and b is the buoyancy acceleration. Once the displacement of fluid particles are known, the centroid of the displaced particles will be determined. The displacement of the fluid particle centroid in the direction of animal motion is defined as Δh, which is used to find ΔPE in equation 4.1.

Using this methodology (equation (6.1)), we can determine how the R_f compares for animals with

varying morphology, size, and swimming modes. Given these observations we will determine which animal swimming characteristic has the greatest impact on R_f by either enhancing or depressing mixing in a stratified fluid. Finally, we will be able to compare the mixing efficiency of swimming animals with physical ocean-mixing processes. The value reported for R_f by swimming *Mastigias sp.* in section 4.3 (and shown in table 4.1) was based on a single data set and animal; we expect variations among animals of the same species as well as across species. Completion of this objective will make biogenic mixing a meaningful process to physical oceanographers. This is especially important when considering the impact biogenic mixing may have on global climate, which requires applicable inputs to oceanographic climate models.

6.3 Effects of Animal Morphology and Swimming Modes on Fluid Transport

To understand how swimming mode, size, and morphology affect animal-induced fluid transport, we will analyze the quantitative flow fields surrounding a swimming animal in the laboratory and in situ. We hope to identify particular animal swimming modes or morphologies that enhance the drift volume and hence transport of fluid in the ocean. From our measurements of jellyfish, we find that the drift effect varies primarily due to animal morphology; the direction of fluid transport is largely due to the swimming mode utilized.

We conducted DPIV measurements of swimming *Phylorhiza sp.* at Marine Biological Laboratories in Woods Hole, MA (figure 6.2). *Phylorhiza sp.* possess similar morphology as *Mastigias sp.* (discussed in chapter 4) as shown in figure 6.2A. Downstream from the bell, a protruding, passive structure called the oral arms serves to filter prey. This structure does not play a role in generating propulsive motion, and instead interacts with vortex rings in the animal's wake. Due to this interaction, the vortex ring impulse is directed at an angle outwards from the body axis instead of directly downstream as normally seen with *Aequorea victoria* and *Aurelia labiata* (see section 3.3). This change in direction of vortex ring impulse serves to reduce the interaction of wake structures

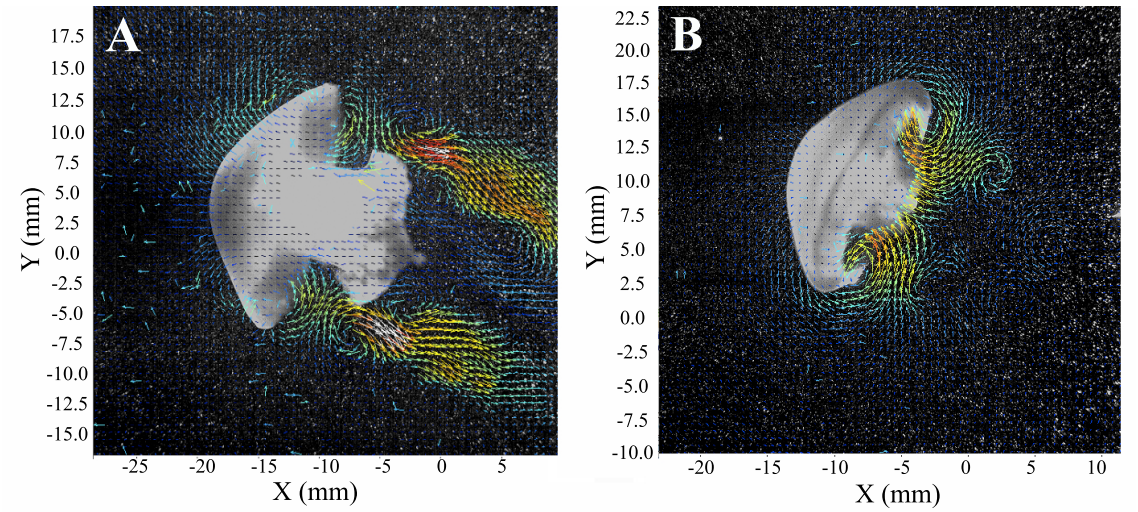

Figure 6.2. Effect of morphology on drift. A, PIV image of flow field generated by swimming *Phylorhiza*, a rhizostome medusae. B, After excising the oral arms, the drift volume is reduced.

with the drift volume located directly behind the swimming animal. The drifting fluid is clearly indicated by the region of flow that is moving in the direction of the animal directly behind the oral arms (figure 6.2A).

Using the same animal, we excised the oral arms and measured the velocity fields surrounding the swimming animal in the same laboratory conditions (figure 6.2B). There is a striking difference in the wake due to the absence of oral arms. It is difficult to identify a drift volume associated with the excised animal that persists after multiple swimming cycles. In addition, the direction of the vortex ring impulse appears to have changed and is directed downstream. Therefore, we may conclude that the presence of the oral arms redirect the wake so as to reduce interference with the drift volume. In order for an animal to have a substantial drift effect, a morphology that prevents interaction of wake structures with the drift volume is necessary. Body orientation during swimming motion may also play a role if the resultant wake is directed away from the drift volume.

The swimming modes selected by an animal during migration will also affect fluid transport. To our knowledge, medusae utilize two different modes of swimming only: rowing and jetting. Rowing is characterized by a long duration contraction phase of the swimming cycle and vortex rings remain stationary relative to a laboratory reference frame (figure 6.3A). Jetting propulsion is characterized

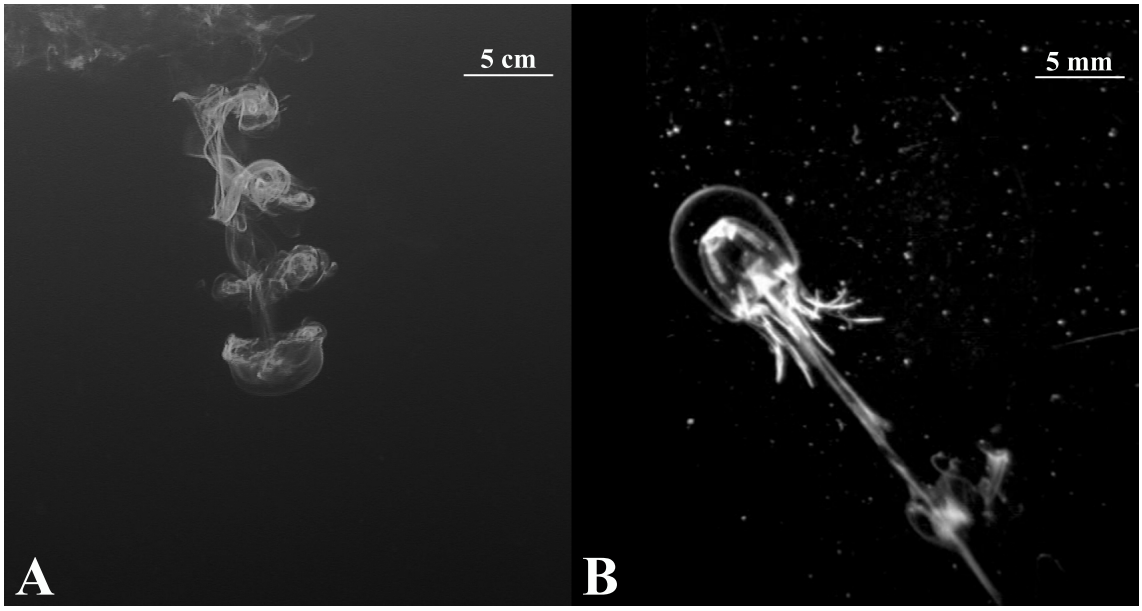

Figure 6.3. Effect of swimming mode on fluid transport, which is a qualitative indicator for mixing efficiency. A, Dye visualization of flow surrounding *Aurelia aurita*, a rowing medusae. B, Dye visualization showing the vortex ring by a medusae utilizing the jetting mode of propulsion.

by short contraction phases and vortex rings that translate at high speeds relative to the laboratory reference frame in the opposite direction of animal motion (figure 6.3B). From our understanding of the drift effect and wake structures corresponding to the two different swimming modes, we expect a larger forward transport of fluid (in the direction of animal motion) if the animal selects the rowing mode. During jetting, the backward motion of fluid may offset the contribution to fluid transport of drift. In addition, animals that utilize the jetting mode of propulsion are characterized by prolate body shapes [24], resulting in a smaller drift effect based on body shape alone (see section 4.3).

The previous conclusions about effects of morphology and swimming mode on drift are based on qualitative observations and few quantitative data. The addition of quantitative metrics that compare animal swimming performance and mixing efficiency are required to support these conclusions. Using these metrics, we can determine whether wake and drift volume interactions depress or enhance overall fluid transport during swimming. From our understanding of wake structures and drift, we can also investigate whether there is a theoretical limit where wake structures dominate fluid transport and mixing over the drift mechanism or vice versa. Completion of this work will

identify animal morphologies and swimming modes that have the greatest or least impact on fluid transport in their environment. Implications of this work can be applied directly to underwater vehicle design and indirectly to ecological impact of certain species of animals.

6.4 Effects of Multiple-Animal Interactions on Drift

In order to determine the importance of biogenic mixing in the global ocean, we need to investigate the effect of multiple-animal interactions on fluid transport and examine the scales at which swimming animals have a significant impact. This effect can either be investigated experimentally, theoretically or numerically given sufficient resources. We have recently become aware of an experimental facility at Woods Hole Oceanographic Institution operated by the Schmitt Fluid Dynamics group in Quissett, MA [111]. The facility includes a tank with vertical dimensions of 10 m and a circular cross section with a diameter of 2 m. The tank has the added capability of being temperature or salt stratified, controlled by internal sensors to set the degree of stratification. Measurements of R_f can be conducted on single or multiple translating bodies in a three-dimensional array configuration. Combining PIV measurements (to measure wake energy due to the translating bodies) and CTD profiles (to determine changes in the vertical density profile), we can experimentally measure R_f due to translating bodies. A more complex measurement would be to replace passive translating bodies with swimming animals.

The interaction of multiple bodies can be investigated theoretically as well. Based on the analytical solution of a sphere moving in either Stokes or potential flow, we can add multiple bodies and vary parameters (such as separation distance and translation speed) to determine their effect on fluid transport and drift. In the other limit (of minimum drift volume), we can simulate a self-propelled swimmer (by modeling a swimming animal by a point force) and add multiple swimmers. These simulations will cover a wide spectrum of animal swimming modes (by varying wake type; passive versus active swimmers) and animal sizes (by varying effects of viscosity; inviscid and non-inertial limits). Finally, we can simulate a stratified fluid using the first-order approximation proposed in section 5.2 to determine whether multiple swimming animals delay the onset of restratification and

allow for complete mixing of stirred fluid by diffusion alone.

Finally, we can use statistical methods to determine the effects of animal schooling characteristics on fluid transport. This analysis will be based on data from the literature on morphology, swimming behavior, and population size of different migrating animals [59, 35]. These migration characteristics will be incorporated into computational models combined with encounter rate theory [136]. Depending on the animal density, swim speed, and motility characteristics, the encounter rate of animals with the drift volume of adjacent animals can impact the time scales at which biogenic mixing is active. Through this research, we can estimate the global impact migrating animals have on their environment with application to climate change and carbon sequestration by the biological pump.

Appendix A

Axisymmetric Assumption for Jellyfish-Generated Flows

To determine the error associated with assuming axisymmetry in jellyfish-generated flows, we will evaluate the continuity equation for a representative data set. In an incompressible flow, the continuity equation can be rewritten such that

$$\nabla \cdot \mathbf{u} = \frac{du}{dx} + \frac{dv}{dy} + \frac{dw}{dz} = 0, \tag{A.1}$$

where u, v, and w correspond to velocity in the x-, y-, and z-directions, respectively. In the case of axisymmetric flow, out-of-plane motions of particles are negligible or $\frac{dw}{dz} \rightarrow 0$. Therefore, in order for a flow to be considered axisymmetric, equation (A.1) can be simplified to

$$\frac{du}{dx} + \frac{dv}{dy} = 0. \tag{A.2}$$

Equation (A.2) must hold for all points if a flow is to be considered axisymmetric. Using the velocity fields acquired from DPIV analysis (figure A.1(a)), equation (A.2) can be evaluated at each data point, resulting in a contour plot with values for continuity (in units of s^{-1}; figure A.1(b)).

To quantify the error associated with using the axisymmetric assumption in real flows, the value of continuity is averaged over the entire field of view, yielding a value of the error for each time step (figure A.1(c)). To be sure, defining the error in this fashion results in a dependence on animal size (since regions of high velocity will correspond to wake structures generated by the swimming animal)

and field of view (the larger the field of view, the smaller the influence of wake structures on the error). Therefore, we expect the error to decrease as animal size (and velocities in wake structures) decreases and field of view increases. We find that the error reaches a maximum near 2.5%, which is well within the error of DPIV measurements.

Finally, the error resulting from the axisymmetric assumption for the entire data set can be found by averaging the error over all time steps (indicated by the black dashed line in figure A.1(c)); the error is approximately 0.2%. Therefore, applying the axisymmetric assumption in flows created by swimming jellyfish is substantiated.

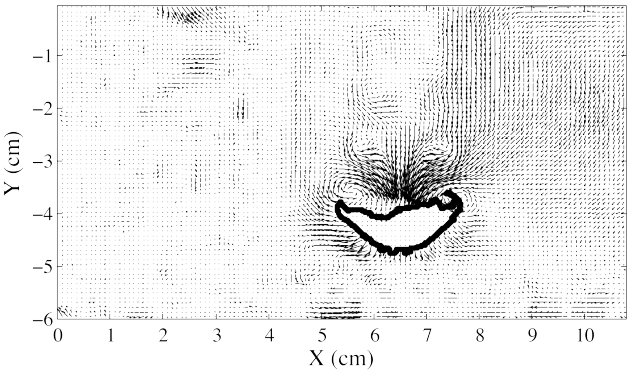

(a)

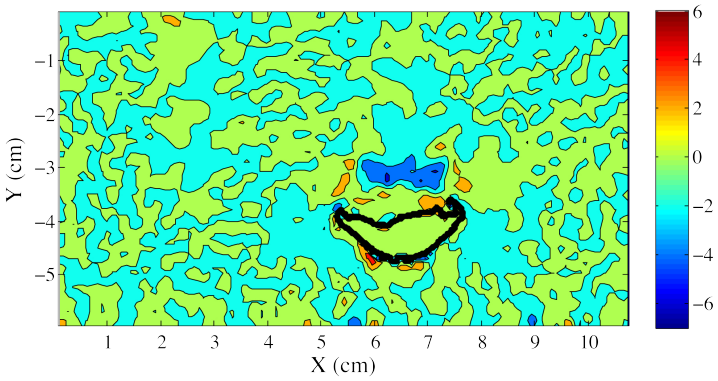

(b)

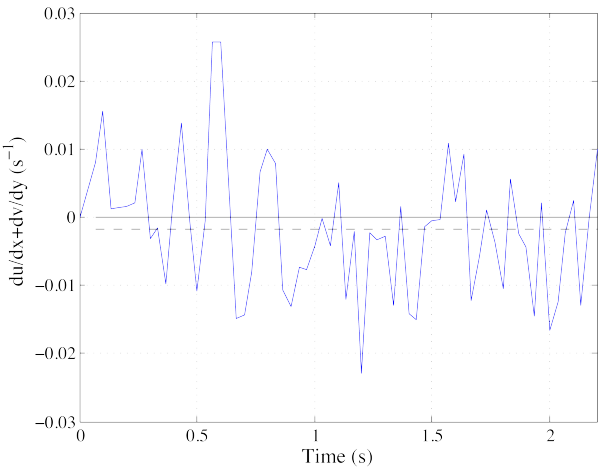

(c)

Figure A.1. Analyzing the axisymmetric assumption using a representative DPIV data set of flow surrounding *Aurelia labiata* in the laboratory. (a) Representative velocity field with the velocity vectors set to zero inside the animal body (indicated by black outline). (b) Contour field showing the value of continuity (equation (A.2)) using the velocity field in (a). (c) The variation of the axisymmetric assumption error (mean value of the continuity equation averaged over the field of view) for multiple swimming cycles of *Aurelia labiata*. Solid black line indicates no error; dashed black line indicates the mean value of error averaged over multiple swimming cycles.

Appendix B

SCUVA Design Iterations

B.1 SCUVA Senior

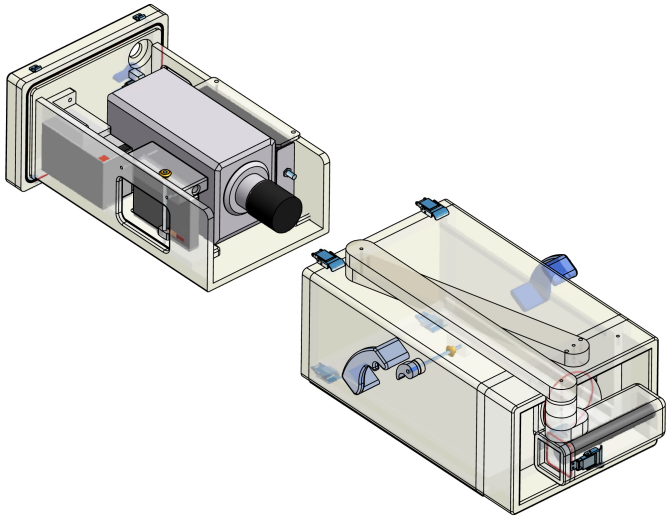

Figure B.1. First-generation design of SCUVA with components, acrylic underwater housings and arm (Sexton Photographics) shown in the laser-stowed position. The components within the camera housing include a high-speed camera (Photron APX-RS), timing electronics (Signal Forge 1000), SLA battery and camera controller (Photron). The waterproof seal is maintained by a single o-ring and four marine-grade clasps. The laser housing is attached to the camera housing via two rigid acrylic arms at the front of the camera housing. Within the laser housing is a solid-state, battery-operated laser (300 mW, 532 nm). The waterproof seal of the laser housing is maintained by a single o-ring and two marine-grade clasps. Drawings are courtesy of Ken Sexton (Sexton Photographics).

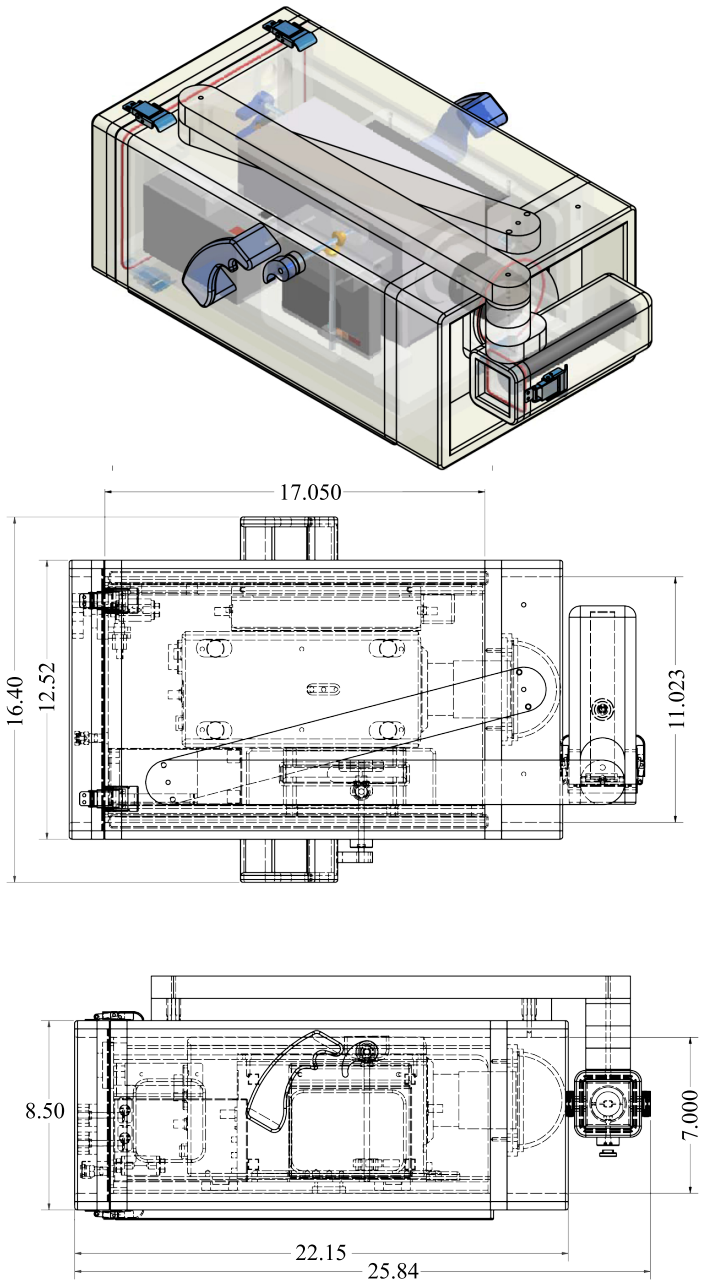

Figure B.2. Dimensions of the underwater camera housing for the first-generation design of SCUVA. Dimensions are shown in inches. Drawings are courtesy of Ken Sexton (Sexton Photographics).

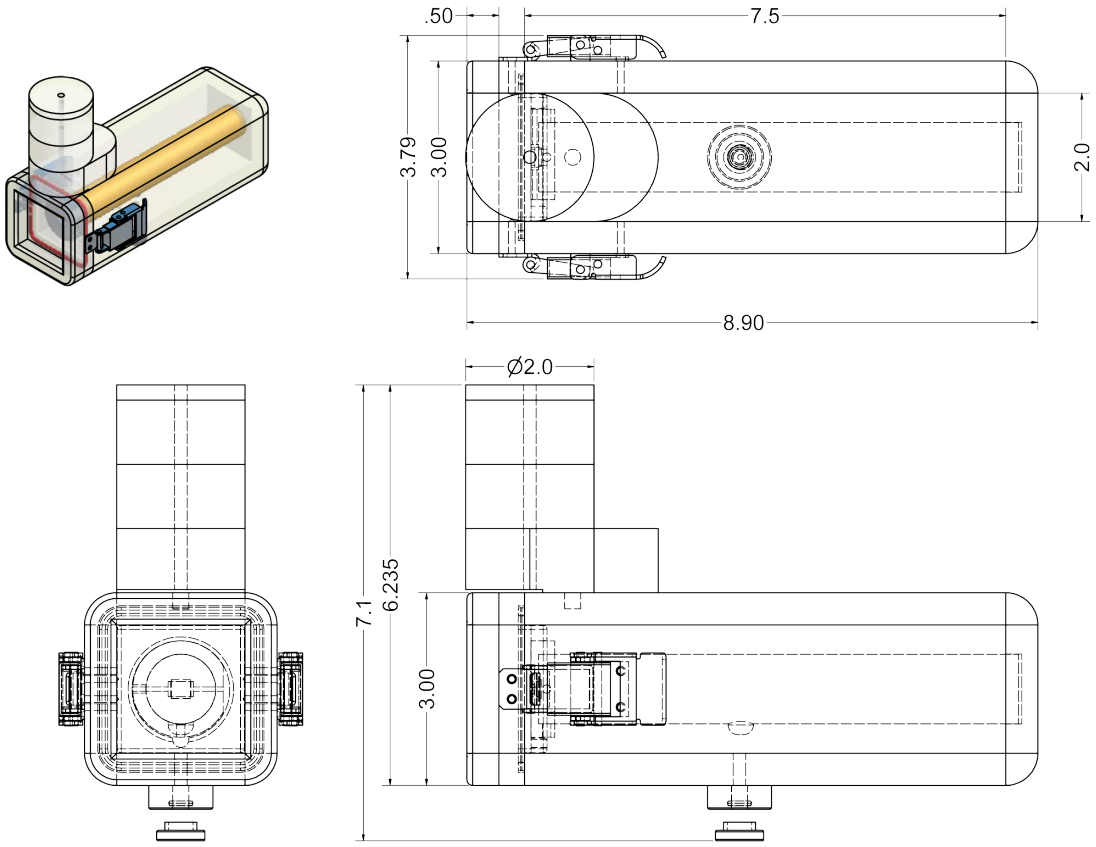

Figure B.3. Dimensions of the underwater laser housing for the first-generation design of SCUVA. Dimensions are shown in inches. Drawings are courtesy of Ken Sexton (Sexton Photographics).

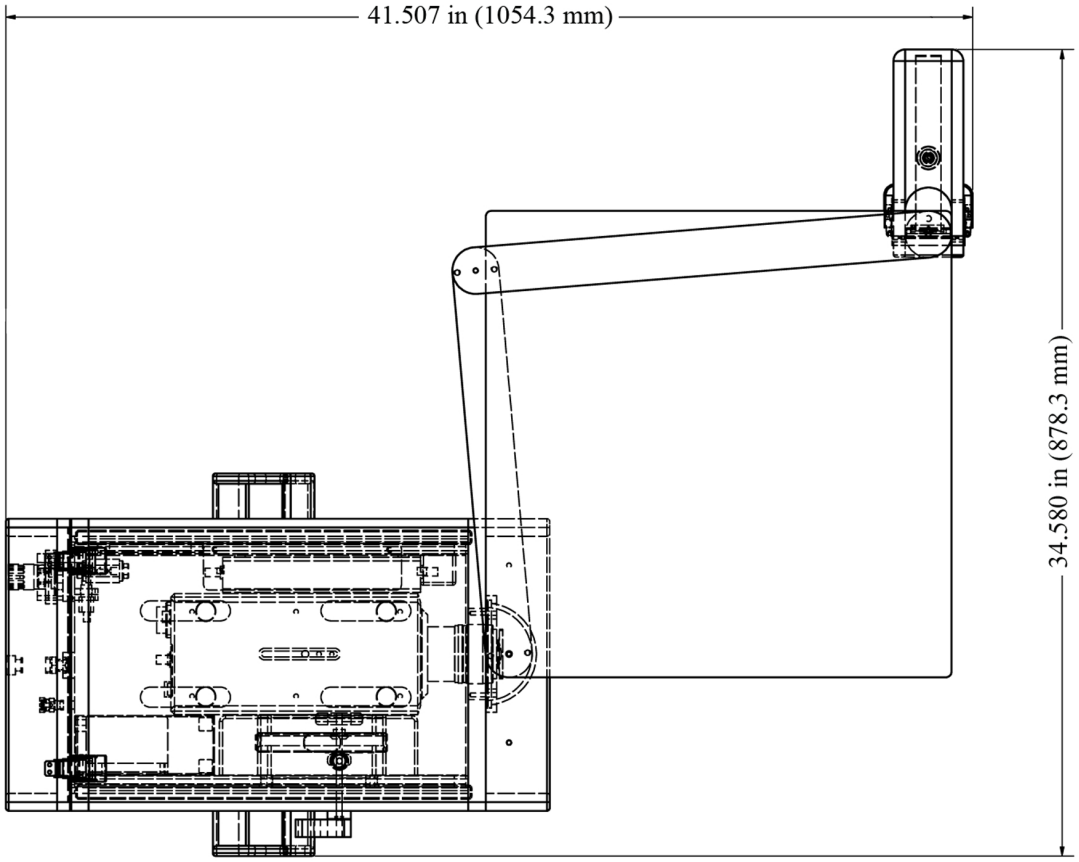

Figure B.4. Dimensions of the attached laser and camera housings for the first-generation design of SCUVA, where the laser housing is in its deployed position. Dimensions are shown in inches (and millimeters in parentheses). Drawings are courtesy of Ken Sexton (Sexton Photographics).

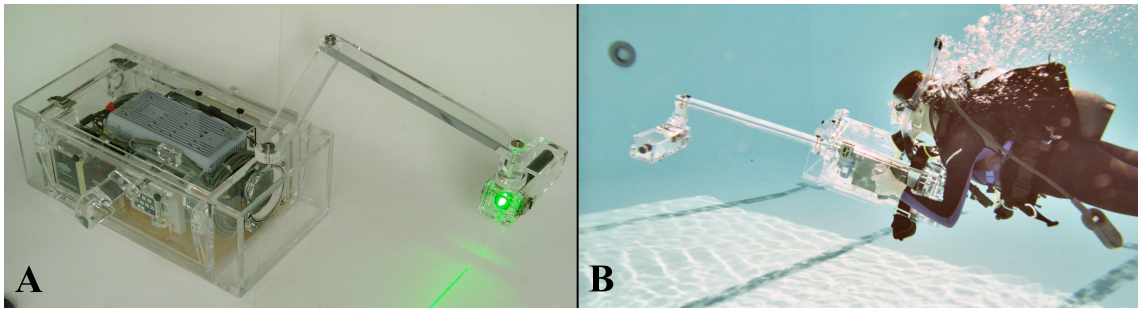

Figure B.5. First-generation design of SCUVA in the laboratory (A, with laser turned on) and during testing at the Caltech pool (B). Scuba diver shown in B is the author. Lead weights were added to the housing to ensure neutral buoyancy and balance during underwater operation.

B.2 SCUVA Junior with *Wickedlaser* Housing

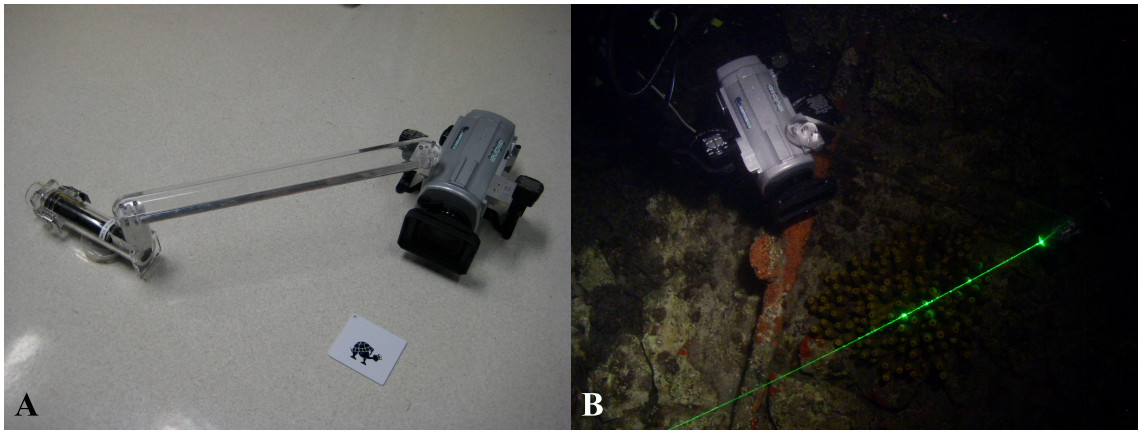

Figure B.6. Second-generation design of SCUVA in the laboratory (A) and in the field (B, Mjlet Lake in Croatia) with the laser turned on. Scuba diver shown in B is the author.

B.3 SCUVA Junior with *Laserglow* Housing

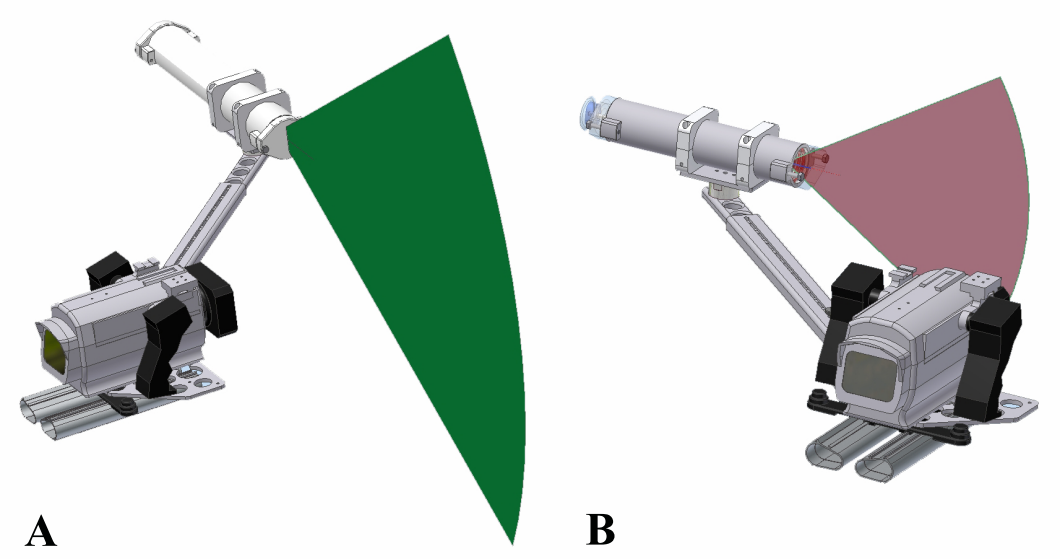

Figure B.7. Diagram showing a third-generation design of SCUVA using a small commercial video camera housing (Amphibico Dive Buddy) and two different laser configurations. The small camera housing is attached to a (A) green and (B) red laser housing containing Hercules and Orion lasers (Laserglow Technologies), respectively. Drawings are courtesy of Ken Sexton (Sexton Photographics).

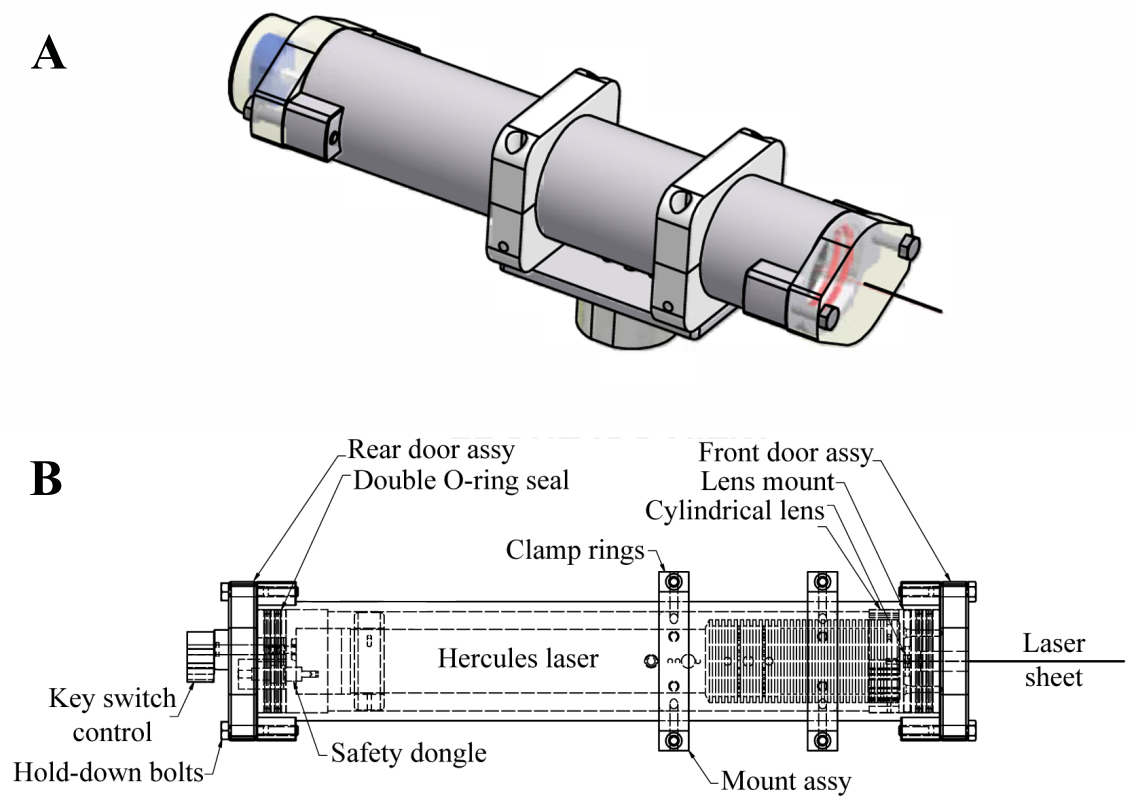

Figure B.8. Diagram of the Hercules laser housing from the (A) ISO and (B) top views. Drawings are courtesy of Ken Sexton (Sexton Photographics).

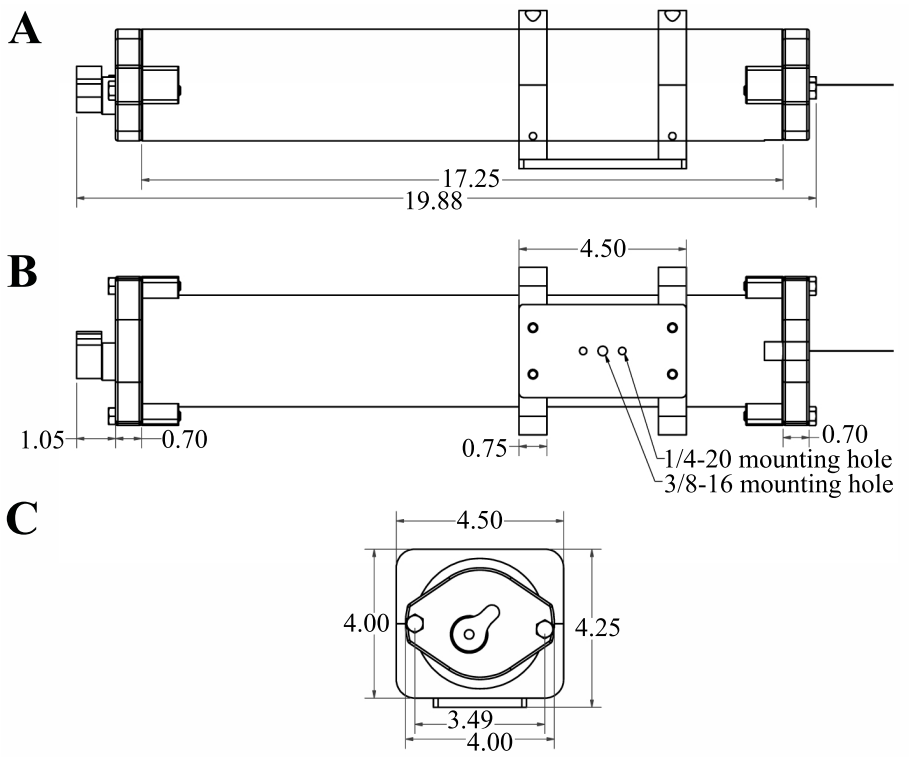

Figure B.9. Dimensions of the Hercules laser housing from the (A) side, (B) top, and (C) front views. Dimensions are shown in inches. Drawings are courtesy of Ken Sexton (Sexton Photographics).

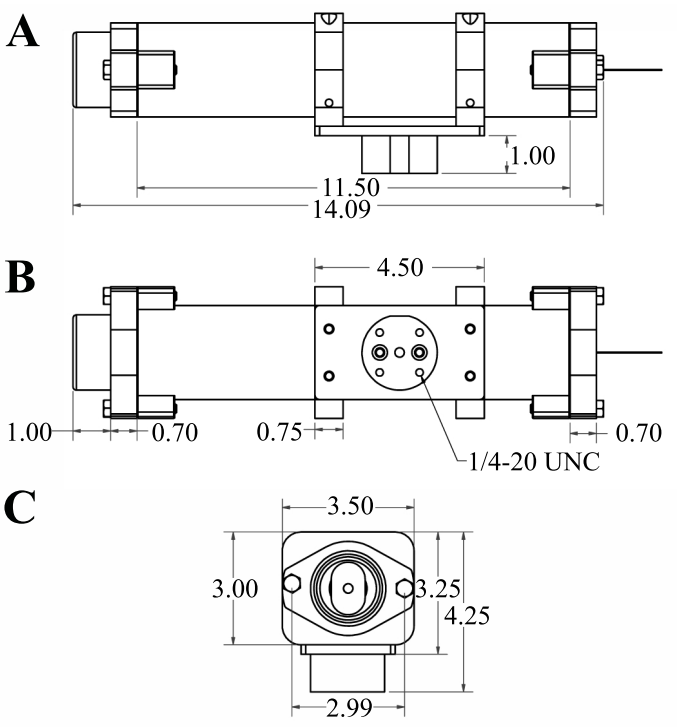

Figure B.10. Dimensions of the Orion laser housing from the (A) side, (B) top, and (C) front views. Dimensions are shown in inches. Drawings are courtesy of Ken Sexton (Sexton Photographics).

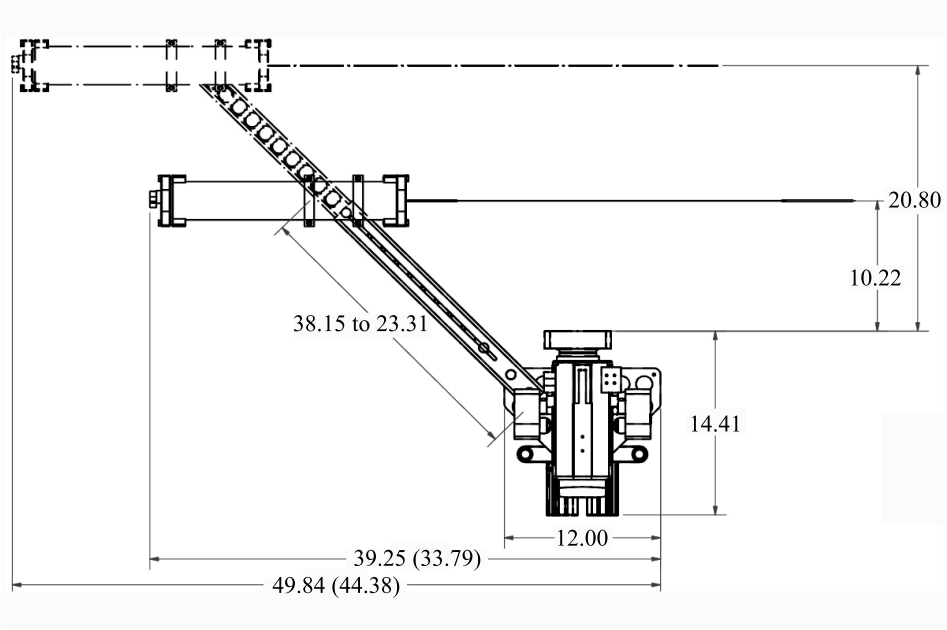

Figure B.11. Dimensions of a third-generation design of SCUVA using a small commercial video camera housing (Amphibico Dive Buddy) and Laserglow laser housings. Dimensions are shown in inches and correspond to the Hercules laser housing (quantities in parentheses correspond to the Orion laser housing). The telescoping arm can be extended from 38.15 to 23.31 in. Drawings are courtesy of Ken Sexton (Sexton Photographics).

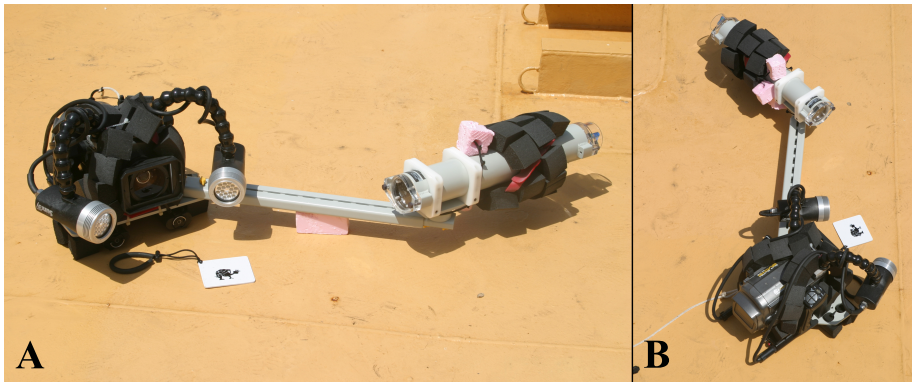

Figure B.12. Third-generation design of SCUVA that incorporates a small commercial video camera housing (Amphibico Dive Buddy). Front (A) and backward views (B) show the arrangement of foam (black and pink cubes) used to obtain neutral buoyancy and balance of the housings underwater.

B.4 SCUVA Autoclave with *Laserglow* Housing

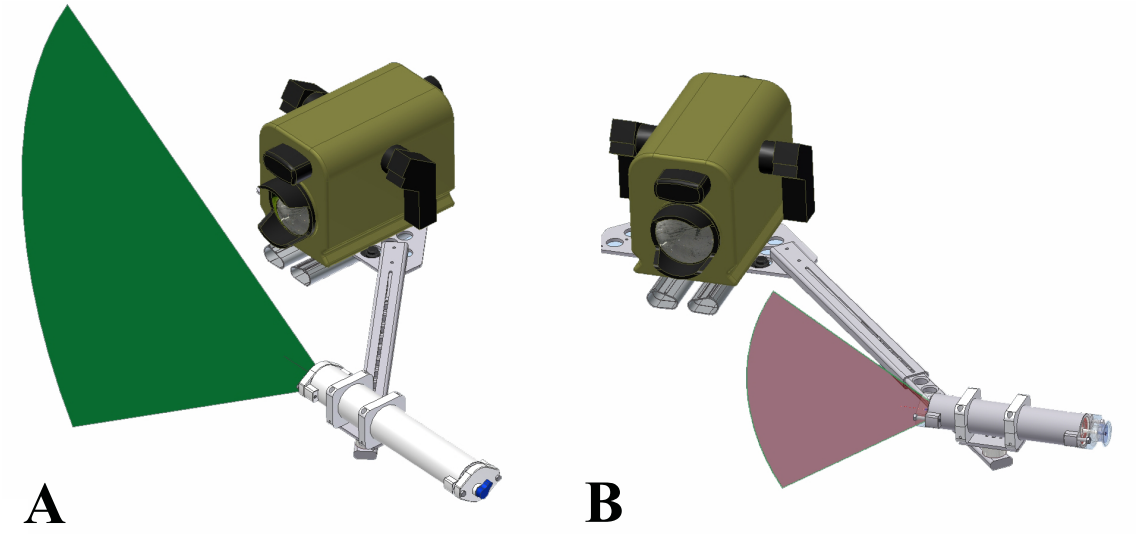

Figure B.13. Diagram showing third-generation design of SCUVA using a large commercial video camera housing (Amphibico Phenom) and two different laser configurations. The large camera housing is attached to a (A) green and (B) red laser housing containing Hercules and Orion lasers (Laserglow Technologies), respectively. Drawings are courtesy of Ken Sexton (Sexton Photographics).

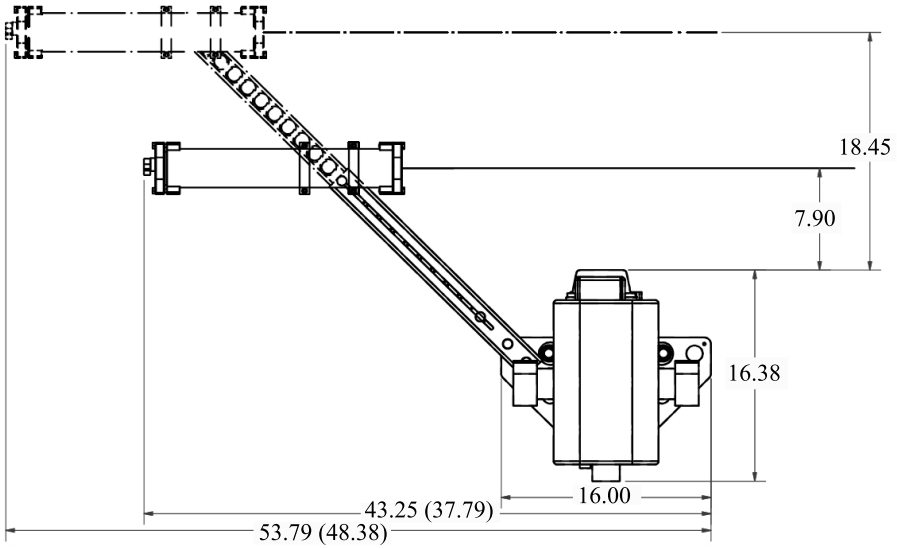

Figure B.14. Dimensions of a third-generation design of SCUVA using a large commercial video camera housing (Amphibico Phenom) and Laserglow laser housings. Dimensions are shown in inches and correspond to the Hercules laser housing (quantities in parentheses correspond to the Orion laser housing). The telescoping arm can be extended from 38.15 to 23.31 in. Drawings are courtesy of Ken Sexton (Sexton Photographics).

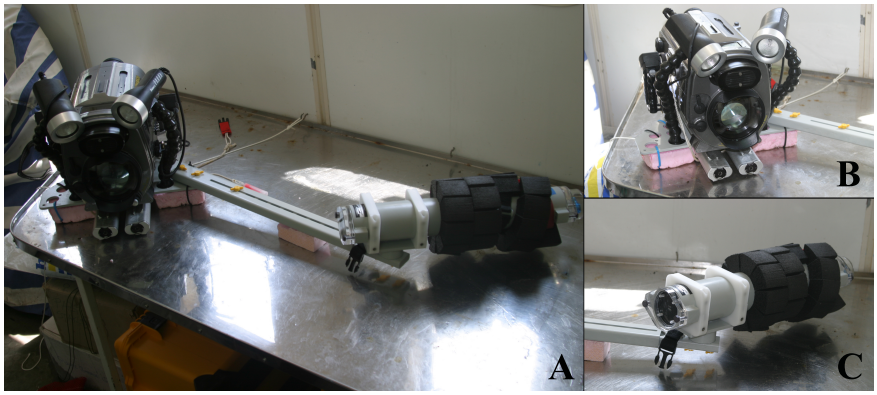

Figure B.15. Third-generation design of SCUVA that incorporates a large commercial video camera housing (Amphibico Phenom model). A, Configuration of apparatus when the laser and camera housings are attached. B and C, The foam arrangement is clearly shown on the camera and laser housings (black and pink cubes), which were used to obtain neutral buoyancy underwater.

Appendix C

Previous Research and Publications

Transport and stirring induced by vortex formation

Shawn Shadden, Kakani Katija, Moshe Rosenfeld, Jerrold E. Marsden and John O. Dabiri (2007). *Journal of Fluid Mechanics*, 593: 315-331.

The purpose of this study is to analyze the transport and stirring of fluid that occurs due to the formation and growth of a laminar vortex ring. Experimental data was collected upstream and downstream from the exit plane of a piston-cylinder apparatus by particle image velocimetry. This data was used to compute Lagrangian Coherent Structures to demonstrate how fluid is advected during the transient process of vortex ring formation. Similar computations were performed from CFD data, which showed qualitative agreement with the experimental results, although the CFD data provides better resolution in the boundary layer of the cylinder. A parametric study is performed to demonstrate how varying the piston-stroke length-to-diameter ratio affects fluid entrainment during formation. Additionally, we study how regions of fluid are stirred together during vortex formation to help establish a quantitative understanding of the role of vortical flows in mixing. We show that identification of the flow geometry during vortex formation can aid in the determination of efficient stirring. We compare this framework with a traditional stirring metric and show that the framework presented in this paper is better suited for understanding stirring/mixing in transient flow problems.

Real-time field measurements of aquatic animal-fluid interactions using a Self-Contained Underwater Velocimetry Apparatus (SCUVA)

Kakani Katija and John O. Dabiri (2008). *Limnology and Oceanography: Methods*, 6: 162-171.

We describe the development of a Self-Contained Underwater Velocimetry Apparatus (SCUVA) that enables a single SCUBA diver to make in situ digital particle image velocimetry (DPIV) measurements of animal-fluid interactions in real time. The device is demonstrated in a study of the dynamics of *Aurelia labiata* jellyfish swimming in the coastal waters of Long Beach, California. We analyze the DPIV measurements by computing the kinetic energy in the flow field induced by an animal's swimming motions. As a proof-of-concept, we compare these results with an existing theoretical model and find that the results are consistent with one another. However, SCUVA provides details regarding the temporal evolution of the energetics during the swimming cycle, unlike the model. These results suggest the usefulness of SCUVA as a method to obtain quantitative field measurements of in situ animal-fluid interactions.

Circulation generation and vortex ring formation in static conic nozzles

Moshe Rosenfeld, Kakani Katija and John O. Dabiri (2008). *Journal of Fluids Engineering*, 131: 091204.

Vortex rings are one of the fundamental flow structures in nature. In this paper, the generation of circulation and vortex rings by a vortex generator with a static converging conic nozzle exit is studied numerically. Conic nozzles can manipulate circulation and other flow invariants by accelerating the flow, increasing the Reynolds number, and by establishing a two-dimensional flow at the exit. The increase in the circulation efflux is accompanied by an increase in the vortex circulation. A novel normalization method is suggested to differentiate between two contributions to the circulation generation: a one-dimensional slug-type flow contribution and an inherently two-dimensional flow contribution. The one-dimensional contribution to the circulation increases with the square of the centerline exit velocity, while the two-dimensional contribution increases linearly with the decrease in the exit diameter. The two-dimensional flow contribution to the circulation production is not limited

to the impulsive initiation of the flow only (as in straight tube vortex generators), but it persists during the entire ejection. The two-dimensional contribution can reach as much as 44% of the total circulation (in the case of an orifice). The present study offers evidences on the importance of the vortex generator geometry, and in particular, the exit configuration on the emerging flow, circulation generation, and vortex ring formation. It is shown that both total and vortex ring circulations can be controlled to some extent by the shape of the exit nozzle.

A viscosity-enhanced mechanism for biogenic ocean mixing

Kakani Katija and John O. Dabiri (2009). *Nature*, 460: 624-626.

Recent observations of biologically generated turbulence in the ocean have led to conflicting conclusions regarding the significance of the contribution of animal swimming to ocean mixing. Measurements indicate elevated turbulent dissipation – comparable with levels caused by winds and tides – in the vicinity of large populations of planktonic animals swimming in concert. However, it has also been noted that elevated turbulent dissipation is by itself insufficient proof of substantial biogenic mixing, since much of the turbulent kinetic energy of small animals is injected below the Ozmidov buoyancy length scale, where it is primarily dissipated as heat by the fluid viscosity before it can affect ocean mixing. Ongoing debate regarding biogenic mixing has focused on comparisons between animal wake turbulence and ocean turbulence. Here, we show that a second, previously neglected mechanism of fluid mixing – first described by Sir Charles Galton Darwin (grandson of the *Origin of Species* author) – is the dominant mechanism of mixing by swimming animals. The efficiency of mixing by Darwin's mechanism is dependent on animal shape rather than fluid length scale and, unlike turbulent wake mixing, is enhanced by fluid viscosity. Therefore, it provides a means of biogenic mixing that can be equally effective in small zooplankton and large mammals. A theoretical model for the relative contributions of Darwinian mixing and turbulent wake mixing is created and validated by in situ field measurements of jellyfish swimming using a newly developed SCUBA-based laser velocimetry device. Extrapolation of these results to other animals is straightforward given knowledge of the animal shape and orientation during vertical migration. Based on calculations of

a broad range of aquatic animal species, we conclude that biogenic mixing via Darwin's mechanism can be a significant contributor to ocean mixing and nutrient transport.

Direct observation of optimal vortex formation by jellyfish

John O. Dabiri, Sean P. Colin, Kakani Katija and John H. Costello. *Journal of Experimental Biology*, 213 (8): 1217-1225.

It is generally accepted that animal-fluid interactions have shaped the evolution of animals that swim and fly. However, the functional ecological advantages associated with those adaptations are currently difficult to predict based on measurements of the animal-fluid interactions. We report the identification of a robust, fluid dynamic correlate of distinct ecological functions in seven jellyfish species that represent a broad range of morphologies and foraging modes. Since the comparative study is based on properties of the vortex wake – specifically, a fluid dynamical concept called optimal vortex formation – and not on details of animal morphology or phylogeny, we propose that higher organisms can also be understood in terms of these fluid dynamic organizing principles. This enables a quantitative, physically-based understanding of how alterations in the fluid dynamics of aquatic and aerial animals throughout their evolution can result in distinct ecological functions.

Comparison of flows generated by *Aequorea victoria*: A coherent structure analysis

Kakani Katija, Sean P. Colin, John O. Dabiri and John H. Costello. *Marine Ecological Progress Series*, submitted.

Cruising-foraging medusae use flow generated during swimming to capture prey. Quantification of their interactions with surrounding fluid is necessary to understand their feeding mechanics and to develop models to predict their predatory impact. The fluid interactions of the cruising-foraging hydromedusa, *Aequorea victoria*, were quantified in the laboratory using digital particle image velocimetry (DPIV) measurements. The laboratory DPIV data supported previous qualitative studies by indicating that regions of maximum flow speed exist adjacent to the bell margin and

in the trailing vortices circulating through the tentacles of the medusae. Velocity vector and shear fields also suggest that the velocity and shear of fluid motion created by *Aequorea victoria* may be more suitable for capturing copepods than previously thought. The measured velocity fields were used to compute finite-time Lyapunov exponent (FTLE) fields, and Lagrangian coherent structures (LCS) were extracted from the FTLE fields. The presence of upstream LCS lobes in the laboratory measurements indicate well-defined regions of fluid that are transported past feeding surfaces and entrained into the wake. These lobes occupy 30% of the fluid located upstream of the medusa's bell. In situ DPIV measurements indicate that ambient flows distort the LCS lobes and affect the ability of cruising-foraging medusae to transport prey to capture surfaces.

Bibliography

[1] Y. C. Agrawal and H. C. Pottsmith. Laser diffraction particle sizing in STRESS. *Cont. Shelf Res.*, 14(10/11):1101–1121, 1994.

[2] M. H. Alford. Improved global maps and 54-year history of wind-work on ocean inertial motions. *Geophys. Res. Letts.*, 30(2166), 2003.

[3] T. K. Barrett and C. W. Van Atta. Experiments on the inhibition of mixing in stably stratified decaying turbulence using laser Doppler anemometry and laser-induced fluorescence. *Phys. Fluids*, 3(5):1321–1332, 1990.

[4] I. K. Bartol, M. R. Patterson, and R. Mann. Swimming mechanics and behavior of the shallow-water brief squid *Lolliguncula brevis*. *J. Exp. Biol.*, 204:3655–3682, 2001.

[5] K. Barz and H. J. Hirsch. Seasonal development of scyphozoan medusae and the predatory impact of *Aurelia aurita* on the zooplankton community in the Bornholm Basin (central Baltic Sea). *Mar. Biol.*, 147:465–476, 2005.

[6] G. K. Batchelor. *An Introduction to Fluid Dynamics*. Cambridge University Press, New York, 1967.

[7] L. Bertuccioli, G. I. Roth, J. Katz, and T. R. Osborn. A submersible particle image velocimetry system for turbulence measurements in the bottom boundary layer. *J. Atm. and Ocean. Tech.*, 16:1635–1646, 1999.

[8] C. Brennen and H. Winet. Fluid mechanics of propulsion by cilia and flagella. *Ann. Rev. Fluid Mech.*, 9:339–398, 1977.

[9] R. E. Britter. *Diffusion and Decay in Stably-Stratified Turbulent Flows. In: Hunt, J.C.R. (Ed.), Turbulence and Diffusion in Stable Environments*. Clarendon, Oxford, 1985.

[10] M. H. Bundy and G. A. Paffenhöfer. Analysis of flow fields associated with freely swimming calanoid copepods. *Mar. Ecol. Prog. Ser.*, 133:99–113, 1996.

[11] D. S. Burdick, D. K. Hartline, and P. H. Lenz. Escape strategies in co-occurring calanoid copepods. *Limnol. Oceanogr.*, 52:2373–2385, 2007.

[12] E. J. Buskey, P. H. Lenz, and D. K. Hartline. Escape behavior of planktonic copepods in response to hydrodynamic disturbances: high speed video analysis. *Mar. Ecol. Prog. Ser.*, 235:135–140, 2002.

[13] J. C. Butcher. *The Numerical Analysis of Ordinary Differential Equations*. Wiley-Interscience, New York, 1987.

[14] K. B. Catton, D. R. Webster, J. Brown, and J. Yen. Quantitative analysis of tethered and free-swimming copepodid flow fields. *J. Exp. Biol.*, 210:299–310, 2007.

[15] A. Chamisso and C. G. Eysenhardt. De animalibus quibusdam e classe Vermium Linneana, in circumnavigatione terrae, auspicante Comite N. Romanzoff duce Ottone de Kotzebue, annis 1815-1818 per acta, observatis. *Nova Acta Acad. Caesar. Leop. Carol.*, 10:345–374, 1821.

[16] A. T. Chwang and T. Y. Wu. Hydromechanics of low Reynolds number flow. Part 2: Singularity method for Stokes flows. *J. Fluid Mech.*, 67:787–815, 1975.

[17] J. Clarke, A. Cotel, and H. Tritico. Development, testing and demonstration of a portable submersible miniature particle imaging velocimetry device. *Meas. Sci. Tech.*, 18:2555–2562, 2007.

[18] S. P. Colin and J. H. Costello. Morphology, swimming performance and propulsive mode of six co-occurring hydromedusae. *J. Exp. Bio.*, 205:427–437, 2002.

[19] S. P. Colin, J. H. Costello, and H. Kordula. Upstream foraging by medusae. *Mar. Ecol. Prog. Ser.*, 327:143–155, 2006.

[20] D. P. Costello and C. Henley. *Methods for Obtaining and Handling Marine Eggs and Embryos*. Marine Biological Laboratory, Woods Hole, MA, 1971.

[21] J. H. Costello and S. P. Colin. Morphology, fluid motion and predation by the scyphomedusa *Aurelia aurita*. *Mar. Biol.*, 121:327–334, 1994.

[22] J. H. Costello and S. P. Colin. Flow and feeding by swimming scyphomedusae. *Mar. Biol.*, 124:399–406, 1995.

[23] J. H. Costello and S. P. Colin. Prey resource utilization by co-occurring hydromedusae from Friday Harbor, Washington, USA. *Limnol. Oceanogr.*, 47:934–942, 2002.

[24] J. H. Costello, S. P. Colin, and J. O. Dabiri. Constraints and consequences in medusan evolution. *Invert. Biol.*, 127:265–290, 2008.

[25] J. P. Crimaldi. Planar laser induced fluorescence in aqueous flows. *Exp. Fluids*, 44(6):851–863, 2008.

[26] J. O. Dabiri. Note on the induced Lagrangian drift and added-mass of a vortex. *J. Fluid Mech.*, 547:105–111, 2006.

[27] J. O. Dabiri, S. P. Colin, and J. H. Costello. Fast-swimming hydromedusae exploit velar kinematics to form an optimal vortex wake. *J. Exp. Biol.*, 209:2025–2033, 2006.

[28] J. O. Dabiri, S. P. Colin, J. H. Costello, and M. Gharib. Flow patterns generated by oblate medusan jellyfish: Field measurements and laboratory analyses. *J. Exp. Biol.*, 208(7):1257–1265, 2005.

[29] J. O. Dabiri and M. Gharib. Fluid entrainment by isolated vortex rings. *J. Fluid Mech.*, 511:311–331, 2004.

[30] J. O. Dabiri, M. Gharib, S. P. Colin, and J. H. Costello. Vortex motion in the ocean: In situ visualization of jellyfish swimming and feeding flows. *Phys. Fluids*, 17(9):091108, 2005.

[31] W. J. A. Dahm and P. E. Dimotakis. Measurements of entrainment and mixing in turbulent jets. *AIAA J.*, 25(9):1216–1223, 1987.

[32] T. L. Daniel. Mechanics and energetics of medusan jet propulsion. *Can. J. Zool.*, 61:1406–1420, 1983.

[33] T. L. Daniel. Unsteady aspects of aquatic locomotion. *Amer. Zoolog.*, 24(1):121–134, 1984.

[34] C. Darwin. Note on hydrodynamics. *Proc. Camb. Phil. Soc.*, 49:342–354, 1953.

[35] W. K. Dewar, R. J. Bingham, R. L. Iverson, D. P. Nowacek, L. C. St. Laurent, and P. H. Wiebe. Does the marine biosphere mix the ocean? *J. Mar. Res.*, 64:541–561, 2006.

[36] N. Didden. On the formation of vortex rings: Rolling-up and production of circulation. *J. App. Math. Phys.*, 30:101–116, 1979.

[37] E. G. Drucker and G. V. Lauder. Locomotor forces on a swimming fish: Three-dimensional vortex wake dynamics quantified using digital particle image velocimetry. *J. Exp. Biol.*, 202:2393–2412, 1999.

[38] I. Eames. The concept of drift and its application to multiphase and multibody problems. *Proc. Roy. Soc. Lond. A*, 361:2951–2965, 2003.

[39] I. Eames, S. E. Belcher, and J. C. R. Hunt. Drift, partial drift and Darwin's proposition. *J. Fluid Mech.*, 275:201–223, 1994.

[40] I. Eames and J. W. M. Bush. Longitudinal dispersion of bodies fixed in a potential flow. *Proc. Roy. Soc. Lond. A*, 455:3665–3686, 1999.

[41] I. Eames, D. Gobby, and S. B. Dalziel. Fluid displacement by Stokes flow past a spherical droplet. *J. Fluid Mech.*, 485:67–85, 2003.

[42] C. Eckart. An analysis of the stirring and mixing processes in incompressible fluids. *J. Mar. Res.*, 7:265–275, 1948.

[43] R. B. Emlet. Flow fields around ciliated larvae: Effects of natural and artificial tethers. *Mar. Ecol. Prog. Ser.*, 63:211–225, 1990.

[44] H. J. S. Fernando. Turbulent mixing in stratified fluids. *Ann. Rev. Fluid Mech.*, 23:455–93, 1991.

[45] A. J. Ferrier, D. R. Funk, and P. J. W. Roberts. Application of optical techniques to the study of plumes in stratified fluids. *Dyn. Atmos. Oceans*, 20(1-2):155–183, 1993.

[46] F. Fish. Comparative kinematics and hydrodynamics of odontocete cetaceans: morphological and ecological correlates with swimming performance. *J. Exp. Biol.*, 201:2867–2877, 1998.

[47] M. D. Ford, J. H. Costello, and E. Klos. Swimming and feeding by the scyphomedusa *Chrysaora quinquecirrha*. *Mar. Biol.*, 129:355–362, 1997.

[48] E. Franco, D. N. Pekarek, J. Peng, and J. O. Dabiri. Geometry of unsteady fluid transport during fluid-structure interactions. *J. Fluid Mech.*, 589:125–145, 2007.

[49] J. Gerritsen and J. R. Strickler. Encounter probabilities and community structure in zooplankton: a mathematical model. *J. Fish Res. Board Can.*, 34:73–82, 1976.

[50] M. A. Green, C. W. Rowley, and G. Haller. Detection of Lagrangian coherent structures in three-dimensional turbulence. *J. Fluid Mech.*, 572:111–120, 2008.

[51] S. Green, A. W. Visser, J. Titelman, and T. Kiørboe. Escape responses of copepod nauplii in the flow field of the blue mussel, *Mytilus edulis*. *Mar. Biol.*, 142:737–742, 2003.

[52] G. Haller. Lagrangian structures and the rate of strain in a partition of two-dimensional turbulence. *Phys. Fluids*, 13(11):3365–3385, 2001.

[53] G. Haller. Lagrangian coherent structures from approximate velocity data. *Phys. Fluids*, 14(6):1851–1861, 2002.

[54] G. Haller. An objective definition of a vortex. *Journal of Fluid Mechanics*, 525:1–26, 2005.

[55] W. M. Hamner, R. W. Gilmer, and P. P. Hamner. The physical, chemical, and biological characteristics of a stratified, saline, sulfide lake in Palau. *Limnol. Oceanogr.*, 27:896–909, 1982.

[56] W. M. Hamner and I. R. Hauri. Long-distance horizontal migrations of zooplankton (scyphomedusae: *Mastigias*). *Limnology and Oceanography*, 26(3):414–423, 1981.

[57] J. E. Higgins, M. D. Ford, and J. H. Costello. Transitions in morphology, nematocyst distribution, fluid motions and prey capture during development of the scyphomedusa *Cyanea capillata*. *Biol. Bull.*, 214:29–41, 2008.

[58] R. Holzman and P. C. Wainwright. How to surprise a copepod: Strike kinematics reduce hydrodynamic disturbance and increase stealth of suction-feeding fish. *Limnol. Oceanogr.*, 54(6):2201–2212, 2009.

[59] M. E. Huntley and M. Zhou. Influence of animals on turbulence in the sea. *Mar. Ecol. Prog. Ser.*, 273:65–79, 2004.

[60] H. E. Huppert and P. C. Manins. Limiting conditions for salt-fingering at an interface. *Deep-Sea Res.*, 20:315–323, 1973.

[61] M. C. Ingham. *The salinity extrema of the world ocean*. PhD thesis, University of Oregon, Corvallis, OR, 1966.

[62] G. N. Ivey and J. Imberger. On the nature of turbulence in a stratified fluid. Part I: The energetics of mixing. *J. Phys. Oceanogr.*, 21:650–658, 1991.

[63] G. N. Ivey and R. I. Nokes. Vertical mixing due to the breaking of critical internal waves on sloping boundaries. *J. Fluid Mech.*, 204:479–500, 1989.

[64] H. Jiang and J. R. Strickler. Copepod flow modes and modulation: A modeling study of the water currents produced by an unsteadily swimming copepod. *Phil. Trans. Roy. Soc. B*, 362:1959–1971, 2007.

[65] K. Katija and J. O. Dabiri. Dynamics of tethered versus free-swimming animals: A wake structure comparison in jellyfish. In *Proc. Amer. Phys. Soc. Div. Fluid Dyn.*, 2006.

[66] K. Katija and J. O. Dabiri. In situ field measurements of aquatic animal-fluid interactions using a self-contained underwater velocimetry apparatus (SCUVA). *Limnol. Oceanogr. Meth.*, 6:162–171, 2008.

[67] K. Katija and J. O. Dabiri. A viscosity-enhanced mechanism for biogenic ocean mixing. *Nature*, 460:624–626, 2009.

[68] J. Katz, P. L. Donaghay, J. Zhang, S. King, and K. Russell. Submersible holocamera for detection of particle characteristics and motions in the ocean. *Deep Sea Res.*, 46:1455–1481, 1999.

[69] T. Kiørboe, E. Saiz, and A. W. Visser. Hydrodynamic signal perception in the copepod *Acartia tonsa*. *Mar. Ecol. Prog. Ser.*, 179:97–111, 1999.

[70] M. A. R. Koehl and J. R. Strickler. Copepod feeding currents: food capture at low Reynolds number. *Limnol. Ocean.*, 26(6):1062–1073, 1981.

[71] M. M. Koochesfahani and P. E. Dimotakis. Mixing and chemical reactions in a turbulent liquid-mixing layer. *J. Fluid Mech.*, 170:83–112, 1986.

[72] E. Kunze. Quantifying salt-fingering fluxes in the ocean. In A. Brandt and J. S. Fernando, editors, *Double-Diffusive Convection*, pages 313–320. AGU Geophysical Monograph, 1995.

[73] E. Kunze. A review of oceanic salt-fingering theory. *Prog. Oceanogr.*, 56:399–417, 2003.

[74] E. Kunze, J. F. Dower, I. Beveridge, R. Dewey, and K. P. Bartlett. Observations of biologically generated turbulence in a coastal inlet. *Science*, 313:1768–1770, 2006.

[75] H. Lamb. *Hydrodynamics*. Dover Publications, New York, 6th edition, 1945.

[76] R. J. Larson. Costs of transport for the scyphomedusae *Stomolophus meleagris* l. agassiz. *Can. J. Zool.*, 65:2690–2695, 1987.

[77] J. R. Ledwell, A. J. Watson, and S. L. Clifford. Evidence for slow mixing across the pycnocline from an open-ocean tracer-release experiment. *Nature*, 364:701–703, 1993.

[78] M. J. Lighthill. Hydromechanics of aquatic animal propulsion. *Ann. Rev. Fluid Mech.*, 1:413–446, 1969.

[79] P. F. Linden. Mixing in stratified fluids. *Geophys. Astrophys. Fluid Dyn.*, 13:3–23, 1979.

[80] P. F. Linden and J. M. Redondo. Molecular mixing in Rayleigh-Taylor instability. Part I: Global mixing. *Phys. Fluids*, 3(5):1269–1277, 1991.

[81] P. F. Linden and T. G. F. Shirtcliffe. The diffusive interface in double-diffusive convection. *J. Fluid Mech.*, 87:417–432, 1978.

[82] P. F. Linden and J. S. Turner. "Optimal" vortex rings and aquatic propulsion mechanisms. *Proc. Roy. Soc. Lond. B*, 271:647–653, 2004.

[83] B. R. MacKenzie and T. Kiørboe. Encounter rates and swimming behavior of pause-travel and cruise larval fish predators in calm and turbulent laboratory experiments. *Limnol. Oceanogr.*, 40:1278–1289, 1995.

[84] M. Mathur, G. Haller, and T. Peacock. Uncovering the Lagrangian skeleton of turbulence. *Phys. Rev. Lett.*, 98(14), 2007.

[85] S. Matsakis and R. J. Conover. Abundance and feeding of medusae and their potential impact as predators on other zooplankton in Bedford Basin (Nova Scotia, Canada) during spring. *Can. J. Fish Aquat. Sci.*, 48:1419–1430, 1991.

[86] C. E. Mills. Diversity of swimming behaviors in hydromedusae as related to feeding and utilization of space. *Mar. Biol.*, 64:185–189, 1981.

[87] J. N. Moum and W. D. Smyth. *Upper Ocean Mixing.* Academic Press, 2001.

[88] W. H. Munk. Abyssal recipes. *Deep Sea Res.*, 13:707–730, 1966.

[89] W. H. Munk and C. Wunsch. Abyssal recipes II: energetics of tidal and wind mixing. *Deep Sea Res.*, 45:1977–2010, 1998.

[90] W. A. M. Nimmo Smith, P. Atsavapranee, J. Katz, and T. R. Osborn. PIV measurements in the bottom boundary layer of the coastal ocean. *Exp. Fluids*, 33:962–971, 2002.

[91] C. O'Farrell and J. O. Dabiri. A Lagrangian approach to identifying vortex pinch-off. *Chaos*, 20:017513, 2010.

[92] E. R. Pardyjak, P. Monti, and H. J. S. Fernando. Flux Richardson number measurements in stable atmospheric shear flows. *J. Fluid Mech.*, 459:307–316, 2002.

[93] J. K. Parrish, S. V. Viscido, and D. Grunbaum. Self-organized fish school: An examination of emergent properties. *Biol. Bull.*, 202:296–305, 2002.

[94] W. R. Peltier and C. P. Caulfield. Mixing efficiency in stratified shear flow. *Annu. Rev. Fluid Mech.*, 35:135–167, 2003.

[95] J. Peng and J. O. Dabiri. An overview of a Lagrangian method for analysis of animal wake dynamics. *J. Exp. Biol.*, To appear, 2007.

[96] J. Peng and J. O. Dabiri. Transport of inertial particles by Lagrangian coherent structures: Application to predator-prey interactions in jellyfish feeding. *J. Fluid Mech.*, 623:75–84, 2009.

[97] J. Peng, J. O. Dabiri, P. G. Madden, and G. V. Lauder. Non-invasive measurement of instantaneous forces during aquatic locomotion: A case study of the bluegill sunfish pectoral fin. *J. Exp. Biol.*, 210:685–698, 2007.

[98] F. Pereira, H. Stuer, E. C. Graff, and M. Gharib. Two-frame 3D particle tracking. *Meas. Sci. Tech.*, 17:1680–1692, 2006.

[99] J. E. Purcell. Predation by the hydromedusa *Aequorea victoria* on fish larvae and eggs at a herring spawning ground in British Columbia. *Can. J. Fish. Aquat. Sci.*, 46:1415–1427, 1989.

[100] J. E. Purcell. Predation by *Aequorea victoria* on other species of potentially competing pelagic hydrozoans. *Mar. Ecol. Prog. Ser.*, 72:255–260, 1991.

[101] J. E. Purcell. Predation on zooplankton by large jellyfish (*Aurelia labiata, Cyanea capillata, Aequorea aequorea*) in Prince William Sound, Alaska. *Mar. Ecol. Prog. Ser.*, 246:137–152, 2003.

[102] J. E. Purcell and J. H. Cowan. Predation by the scyphomedusan *Chrysaora quinquecirrha* on *Mnemiopsis leidyi* ctenophores. *Mar. Ecol. Prog. Ser.*, 128:63–70, 1995.

[103] K. A. Raskoff. Foraging, prey capture, and gut contents of the mesopelagic narcomedusae *Solmissus sp.* (Cnidaria: Hydrozoa). *Mar. Biol.*, 141:1099–1107, 2002.

[104] C. R. Rehmann and J. R. Koseff. Mean potential energy change in stratified grid turbulence. *Dyn. Atmos. Oceans*, 37:271–294, 2004.

[105] V. Romkedar, A. Leonard, and S. Wiggins. An analytical study of transport, mixing and chaos in an unsteady vortical flow. *J. Fluid Mech.*, 214:347–394, 1990.

[106] K. Schmidt-Nielsen. Locomotion: Energy cost of swimming, flying, and running. *Science*, 177:222–228, 1972.

[107] R. W. Schmitt. The characteristics of salt fingers in a variety of fluid systems including stellar interiors, liquid metals, oceans and magmas. *Phys. Fluids*, 26:2373–2377, 1983.

[108] R. W. Schmitt. On the density ratio balance in the Central Water. *J. Phys. Oceanogr.*, 20(6):900–906, 1990.

[109] R. W. Schmitt. Double diffusion in oceanography. *Ann. Rev. Fluid Mech.*, 26:255–285, 1994.

[110] R. W. Schmitt, J. R. Ledwell, E. T. Montgomery, K. L. Polzin, and J. M. Toole. Enhanced diapycnal mixing by salt fingers in the thermocline of the tropical Atlantic. *Science*, 308:685–688, 2005.

[111] R. W. Schmitt, R. C. Millard, J. M. Toole, and W. D. Wellwood. A double-diffusive interface tank for dynamic-response studies. *J. Mar. Res.*, 63:263–289, 2005.

[112] S. C. Shadden. *A dynamical systems approach to unsteady systems.* PhD thesis, California Institute of Technology, 2006.

[113] S. C. Shadden, J. O. Dabiri, and J. E. Marsden. Lagrangian analysis of fluid transport in empirical vortex ring flows. *Phys. Fluids*, 18(4):047105, 11, 2006.

[114] S. C. Shadden, K. Katija, M. Rosenfeld, J. E. Marsden, and J. O. Dabiri. Transport and stirring induced by vortex formation. *J. Fluid Mech.*, 2007.

[115] S. C. Shadden, F. Lekien, and J. E. Marsden. Definition and properties of Lagrangian coherent structures from finite-time Lyapunov exponents in two-dimensional aperiodic flows. *Phys. D*, 212(3-4):271–304, 2005.

[116] A. J. Smits. *A Physical Introduction to Fluid Mechanics.* John Wiley and Sons, New York, 2000.

[117] L. St. Laurent and C. Garrett. The role of internal tides in mixing the deep ocean. *J. Phys. Oceanogr.*, 32:2882–2899, 2002.

[118] J. V. Steinbuck, C. D. Troy, P. J. Franks, E. Karakoylu, J. S. Jaffe, S. G. Monismith, and A. R. Horner. Small-scale turbulence measurements with a free-falling DPIV profiler. In *Proc. Amer. Geophys. Un.*, 2004.

[119] M. E. Stern. The "salt fountain" and thermohaline convection. *Tellus*, 12:172–175, 1960.

[120] E. J. Strang and H. J. S. Fernando. Entrainment and mixing in stratified shear flows. *J. Fluid Mech.*, 428:349–386, 2001.

[121] J. R. Strickler. Calanoid copepods, feeding currents, and the role of gravity. *Science*, 218:158–160, oct 1982.

[122] C. L. Suchman and B. K. Sullivan. Vulnerability of the copepod *Acartia tonsa* to predation by the scyphomedusa, *Chrysaora quinquecirrha*. *Mar. Biol.*, 132:237–245, 1998.

[123] C. L. Suchman and B. K. Sullivan. Effect of prey size on vulnerability of copepods to predation by the scyphomedusae *Aurelia aurita* and *Cyanea* sp. *J. Plank. Res.*, 22(12):2289–2306, 2000.

[124] B. K. Sullivan, J. R. Garcia, and G. Klein-MacPhee. Prey selection by the scyphomedusan predator *Aurelia aurita*. *Mar. Biol.*, 121:335–341, 1994.

[125] K. Taira and T. Colonius. The immersed boundary method: A projection approach. *J. Comput. Phys.*, 225:2118–2137, 2007.

[126] G. I. Taylor. Analysis of the swimming of microscopic organisms. *Proc. Roy. Soc. London A*, 209:447–461, 1951.

[127] H. Tennekes and J. L. Lumley. *A First Course in Turbulence*. MIT Press, Cambridge, 1972.

[128] S. A. Thorpe. *The Turbulent Ocean*. Cambridge University Press, Cambridge, 2005.

[129] J. Titelman and L. J. Hansson. Feeding rates of the jellyfish *Aurelia aurita* on fish larvae. *Mar. Biol.*, 149:297–306, 2006.

[130] J. S. Turner and H. Stommel. A new case of convection in the presence of combined vertical salinity and temperature gradients. *Proc. Natl. Acad. Sci.*, 52:49–53, 1964.

[131] E. D. Tytell and G. V. Lauder. The hydrodynamics of eel swimming. *J. Exp. Biol.*, 207:1825–1841, 2004.

[132] G. K. Vallis. *Atmospheric and Oceanic Fluid Dynamics*. Cambridge University Press, Cambridge, 2006.

[133] J. J. Videler, E. J. Stamhuis, U. K. Müller, and L. A. van Duren. The scaling and structure of aquatic animal wakes. *Integr. Compar. Biol.*, 42:988–996, 2002.

[134] M. Viitasalo, T. Kiørboe, J. Flinkman, L. W. Pederson, and A. W. Visser. Predation vulnerability of planktonic copepods: consequences of predator foraging strategies and prey sensory abilities. *Mar. Ecol. Prog. Ser.*, 175:129–142, 1998.

[135] A. W. Visser. Biomixing of the oceans? *Science*, 316:838–839, 2007.

[136] A. W. Visser and T. Kiørboe. Plankton motility patterns and encounter rates. *Oecol.*, 148:538–546, 2006.

[137] S. Vogel. Flight in *Drosophila*: I. Flight performance of tethered flies. *J. Exp. Biol.*, 44:567–578, 1966.

[138] S. I. Voropayev and Y. D. Afanasyev. *Vortex structures in a stratified fluid: Order from chaos*. Chapman and Hall, London, 1994.

[139] R. J. Waggett and E. J. Buskey. Calanoid copepod escape behavior in response to a visual predator. *Mar. Biol.*, 150:599–607, 2007.

[140] C. E. Willert and M. Gharib. Digital particle image velocimetry. *Exp. Fluids*, 10(4):181–193, 1991.

[141] C. Wunsch. The work done by the wind on the oceanic general circulation. *J. Phys. Oceanogr.*, 28:2332–2340, 1998.

[142] C. Wunsch and R. Ferrari. Vertical mixing, energy and the general circulation of the oceans. *Annu. Rev. Fluid Mech.*, 36:281–314, 2004.

[143] J. Yen, J. Brown, and D. R. Webster. Analysis of the flow field of the krill, *Euphausia Pacifica*. *Mar. Fresh. Behav. Physiol.*, 36(4):307–319, 2003.